NANO LETTERS

pubs.acs.org/NanoLett Letter

Polygonal Wrinkles in a Soft Solidified Droplet

Li Chen, Cheng Cao, Yuqi Li, Wenna Wu, Man Hu,* Qi Tong,* and Daosheng Deng*

Cite This: *Nano Lett.* 2025, 25, 9899−9903 Read Online

ACCESS | Metrics & More | Article Recommendations | Supporting Information

ABSTRACT: The widespread occurrence of liquid freezing has profound implications for materials science, advanced manufacturing, and the global climate. Emerging from the intricate interplay of fluid dynamics, heat transfer, and phase change, recently, a captivating array of artistic and elegant patterns has been revealed. However, the solidified liquid component generally displays a pronounced resistance to deformation, thereby hindering the critical mechanical coupling inherently associated with thin films and soft materials. In this study, by investigating a hexadecane droplet impacting an aluminum substrate under strong supercooling conditions, we observe that this soft solidified droplet undergoes self-folding, followed by polygonal wrinkling due to Gauss's theorema egregium. These polygonal wrinkles of the submillimeter-thin film experience a striking sequential morphological transformation, characterized by a diminishing edge number, transitioning from octagonal to heptagonal, ultimately culminating in a tetragonal configuration. Both scaling analysis and numerical simulations demonstrate excellent agreement with the observed polygonal wrinkles.

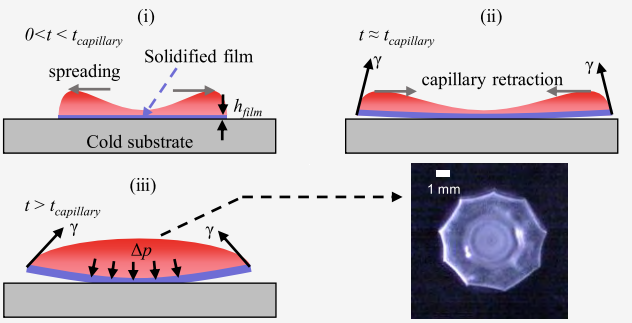

KEYWORDS: *Soft solidified droplet, Polygonal wrinkles, Supercooling, Elasto-capillarity effect*

Downloaded via FUDAN UNIV on June 25, 2025 at 07:54:22 (UTC).
See https://pubs.acs.org/sharingguidelines for options on how to legitimately share published articles.

Liquid freezing in nature is closely associated with global climate change[1] and plays a crucial role in a broad range of technologies, including cryobiology,[2] the food industry,[3] and materials science.[4] As exemplified by Prince Rupert's drops in the 17th century, also known as Batavian tears, red-hot droplets of molten glass were released into water, subsequently forming tadpole-shaped pieces of glass that were subjected to supercooling. Their extraordinary mechanical properties, featuring a strong head and a fragile tail, intrigued England's King Charles II, to whom Prince Rupert of Germany presented these glass drops.[5−8]

Due to the strong multiphysical coupling across multiple length and time scales, various complex patterns have been identified in the morphology of an impacted frozen droplet.[9−11] During this process, the delicate fluid−thermal coupling of hydrodynamic flow, capillary effects, and phase transitions gives rise to a host of fascinating behaviors, including tip singularities,[12] hierarchical cracking patterns to release the thermal contraction stress,[13] delamination and peeling once thermal stress overcoming adhesive stress,[14] and self-lifting droplets driven by an internal solutal Marangoni flow.[15]

Alternatively, the fluid−mechanical coupling, as exemplified by the intricate interplay between droplets and sheets, arises from the interaction between surface tension and elasticity.[16−18] This coupling can generate fascinating elastocapillarity phenomena, such as capillary origami during spontaneous wrapping of a droplet with an elastic sheet,[19] capillary wrinkling by a floating droplet on a nanoscale-thickness polymer film,[20] capillary wrapping with a near-perfect seam.[21]

In this work, by impacting a hexadecane droplet onto a supercooled substrate, we observe self-folding and subsequent polygonal wrinkling in the soft solidified droplet. We find that at strong supercooling, the solidified film, which is tens of micrometers thick, is peeled off from the substrate at the onset of the retraction stage or at the capillary time scale by overcoming adhesive stress. Due to the elastocapillary effect, this thin film is subjected to buckling instability, forming polygonal wrinkling patterns. The number of edges in these patterns gradually diminishes over time. Both scaling analysis and numerical simulations show remarkable agreement with experimental observations.

Observation of Self-Folding. A hexadecane droplet ($C_{16}H_{34}$, freezing temperature $T_{freezing}$ = 18.0 °C, the diameter of D_0 = 2.8 mm, or the volume of V_0 = 11.5 μL) was generated by a capillary needle at room temperature and released from an initial falling height H_0. Then the droplet at a velocity $u_0 \sim (2gH_0)^{1/2}$ impacts a cold aluminum substrate $T_{sub} \in (-10, -60)$ °C, corresponding to supercooling $\Delta T = (T_{freezing} - T_{sub}) \in (28, 78)$ °C (Supplementary Note S1).

Received: December 20, 2024
Revised: June 3, 2025
Accepted: June 6, 2025
Published: June 11, 2025

ACS Publications © 2025 American Chemical Society

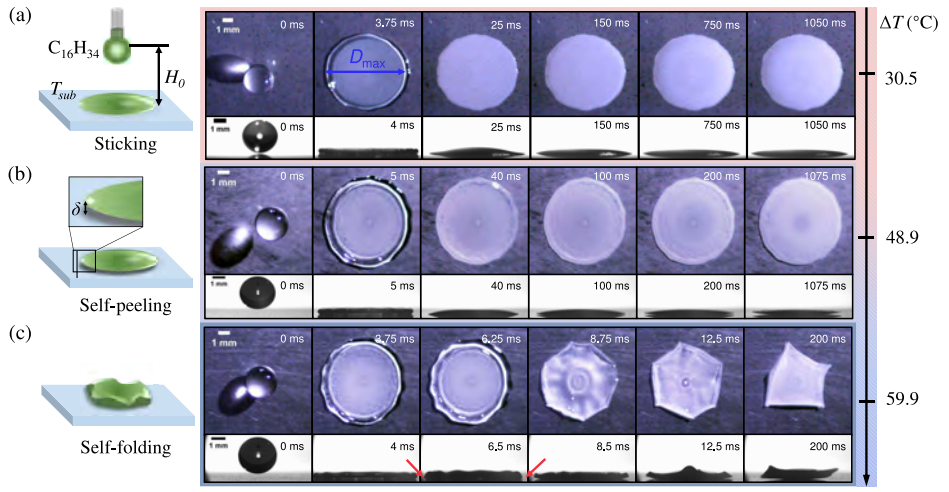

Figure 1. Solidification patterns as a function of ΔT for a hexadecane droplet falling from H_0 = 10 cm. (a) Sticking pattern at weak supercooling of ΔT = 30.5 °C at T_{sub} = − 12.5 °C. (b) Self-peeling pattern at moderate supercooling of ΔT = 48.9 °C at T_{sub} = − 30.9 °C. (c) Self-folding pattern with the distinctive polygonal configuration at strong supercooling of ΔT = 59.9 °C at T_{sub} = −41.9 °C. The blue line shows the maximum spreading diameter D_{max}, while the red arrows indicate the onset of self-folding.

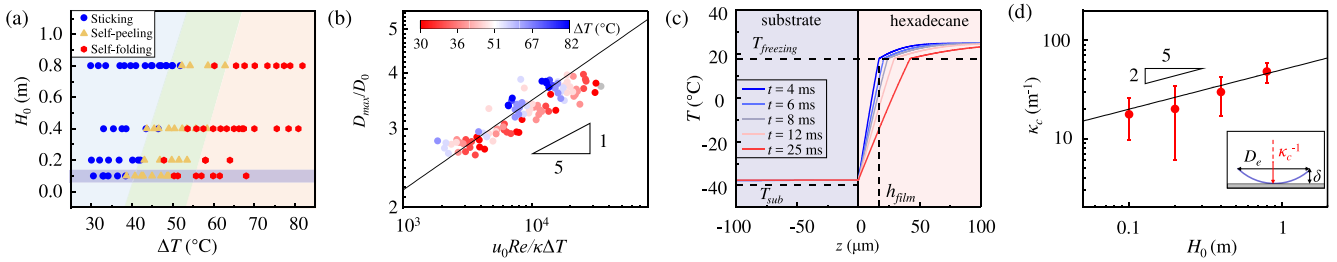

Figure 2. Phase diagram of solidified pattern. (a) Phase diagram of sticking, self-peeling, and self-folding depending on H_0 and ΔT. (b) 1/5 scaling law of D_{max}/D_0 in eq 1. (c) Temperature profile calculated from the 1D two-phase Stefan model. (d) 2/5 scaling law of the bending curvature κ_c with H_0 in eq 2; the inset is the geometric sketch.

Figure 1 presents the fast-speed images of the solidification pattern as a function of supercooling. At weak supercooling ΔT = 30.5 °C or T_{sub} = −12.5 °C (Figure 1a), during its spreading stage, the droplet extends radially outward, until reaching the maximum spreading diameter ($D_{max} = 2R_{max}$). Meanwhile, a thin solidified film of hexadecane is gradually formed by contacting the cold substrate. Afterward during the retraction stage, solidification along the vertical direction continues, and the upper residual liquid contracts inward to the center. Eventually, the thickness of the solidified film increases, but the solidified film remains stuck to the substrate due to the interfacial adhesive stress, leading to the sticking pattern similar to the frozen pattern of the impacting water droplet[22,23] (Supplementary Movie 1).

At moderate supercooling of ΔT = 48.9 °C at T_{sub} = −30.9 °C (Figure 1b), the effect of thermal stress mismatch within the solidifying film is significantly magnified when subjected to vertical cooling and a temperature gradient, arising from the thermal contraction in the solidified film. From the side-view snapshot at t = 100 ms, the film starts to peel off, and then gradually the air gap (δ) between the deformed edge of the film and the substrate further widens (Supplementary Movie 2). Thus, by overcoming the adhesion stress, the solidified hexadecane droplet detaches from the substrate to release the stress and form the self-peeling pattern, in a fashion similar to a metal droplet or water droplet.[14,24]

However, at strong supercooling of ΔT = 59.9 °C at T_{sub} = −41.9 °C (Figure 1c), although the spreading stage is similar to that in the sticking and self-peeling patterns, the distinctive behavior of the self-folding pattern is observed during the retraction stage (Supplementary Movie 3). At the onset of retraction of the residual liquid film at t = 6.5 ms, the edge or outer rim of the film bends and lifts off, as indicated by the red arrows from the side-view snapshot. Then, as the residual liquid film continues to retract inward, the bottom film is further pulled up and eventually encounters the self-folding process, resulting in an intriguing wrinkle morphology.

From the top-view snapshots (Figure 1c), the rims of the solidified film display polygonal transformation with a decrease in the number of edges (N), from an octagon shape (N = 8) at t = 8.5 ms, to hexagon (N = 6) and quadrilateral (N = 4) contours at t = 12.5 ms and t = 200 ms, respectively. Further, this large detachment (δ) between the solidified film and the substrate is validated from the side-view snapshots, confirming the self-folding.

Phase Diagram. By investigation of a wide range of physical parameters of the initial falling height H_0 and supercooling ΔT in experiments, a phase diagram (Figure 2a) is established for the three solidification patterns. As the degree of supercooling increases for a given H_0, the pattern transition progresses through sticking, self-peeling, and self-folding stages.

We perform scaling analysis of D_{max} during the spreading stage, which is dominated by the inertia-viscous effect, $D(t) \sim Re^{1/6}(u_0D_0^5)^{1/6}t^{1/6}$,[25,26] where $Re = \rho u_0 D_0/\mu$ is the Reynolds number and ρ the density and μ the viscosity of

https://doi.org/10.1021/acs.nanolett.4c06529
Nano Lett. 2025, 25, 9899−9903

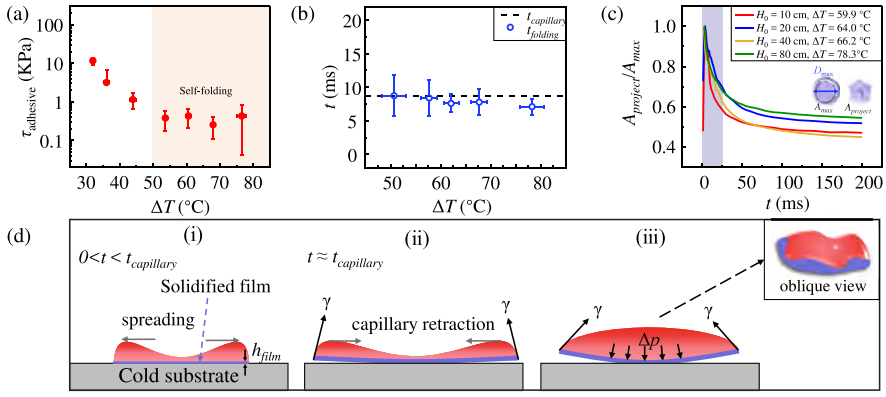

Figure 3. Self-folding mechanism. (a) The measured adhesive stress ($\tau_{adhesive}$) as a function of ΔT, and the occurrence of self-folding at strong supercooling. (b) The self-folding time scale aligning with the capillary time scale $t_{folding} \simeq t_{capillary}$ of eq 4. (c) Time-dependent $A_{project}/A_{max}$ indicating the fast self-folding and subsequently the slow transition of polygonal wrinkling. (d) Sketch of (i) spreading stage with the increased h_{film} with time, (ii) peeling at the instance of retraction stage, and (iii) the subsequent folding and wrinkling by the elasto-capillarity effect.

hexadecane, respectively. D_{max} is reached when the spreading front is arrested, which occurs once the velocity of the freezing front $v_{freezing} = \kappa\Delta T$ (κ = 0.011 m ·s^{-1} ·K^{-1} for the kinetic coefficient)[25] matches the velocity at the contact line $v_{cl} \sim D(t)/t \sim Reu_0[D_0/D(t)]^5|_{D(t)=D_{max}}$.[26] Then the following scaling is obtained,

$$\frac{D_{max}}{D_0} \sim \left(\frac{u_0 Re}{\kappa \Delta T}\right)^{1/5} \tag{1}$$

Indeed, as shown in Figure 2b, all experimental data for ΔT = 20−82 °C and H_0 = 10, 20, 40, and 80 cm collapse on a single master line with 1/5 scaling.

Self-Peeling. At moderate supercooling, the bottom solidified film is detached from the substrate around 100 ms during the late retraction stage (Figure 1b). The thickness of solidified film (h_{film}) grows with time, $h_{film}(t) \sim (D_s t)^{1/2} \sim (\Delta T t)^{1/2}$,[15] where $D_s = 2k_s\Delta T/(\rho_s L)$ is a diffusion coefficient, k_s and ρ_s are the thermal conductivity and the density of the solidified liquid, respectively, L is the latent heat of solidification per unit mass, and ΔT is the degree of supercooling. Based on the 1D theory of the two-phase Stefan model (Figure 2c, Supplementary Note S4), h_{film} reaches tens of micrometers within tens of milliseconds, and the temperature profile has a nearly linear distribution within the solidified film.[13,22]

We perform scaling analysis for the bending curvature of the self-peeling due to thermal stresses. By simplifying the solidified film as a free thin disk subjected to a constant temperature gradient, the thermal elastic moment density can be obtained,[27] $M_{thermal} \sim EH_{film}^2(\alpha\Delta T)$, where E and α are Young's elastic modulus and the thermal expansion coefficient, while the film thickness at the instant of peeling $H_{film} \sim D_0^3/D_{max}^2 \sim (H_0/\Delta T)^{-2/5}$ from eq 1. By combining $M_{thermal}$ with the bending stiffness $B \sim EH_{film}^3$, the bending curvature (κ_c) is expressed as below,

$$\kappa_c \sim M_{thermal}/B \sim \alpha\Delta T/H_{film} \sim \Delta T^{3/5} H_0^{2/5} \tag{2}$$

Indeed, this 2/5 power law is comparable with the experimental data for the curvature as a function of H_0 (Figure 2d). Here the bending curvature in experiments is directly calculated from the side-view profile (the inset of Figure 2d), $\kappa_c = 8\delta/(4\delta^2 + D_e^2)$, where D_e is the diameter of the outer edge or rim and δ is the vertical distance between the outer edge and the substrate.[24]

Self-Folding Mechanism. The self-folding occurs around 10 ms at strong supercooling (Figure 1c), which is much faster than the occurrence time scale of self-peeling around 100 ms. In both cases, the thermal-elastic stresses within the solidified film [$\sigma_{thermal} \sim E(\alpha\Delta T)^2$] need to overcome the adhesive stress [$\tau_{adhesive}(T)$] between the solidified film and solid substrate,[14]

$$\sigma_{thermal} > \tau_{adhesive}(T) \tag{3}$$

As shown from the measured adhesive stress, $\tau_{adhesive}(T)$, between the solid hexadecane and aluminum substrate (Figure 3a, Supplementary Note S2), as supercooling level ΔT increases from 30 to 50 °C, the adhesion strength is reduced dramatically with 2 orders of magnitude, from 10 to 0.1 KPa. Hence, at strong supercooling (ΔT > 50 °C), $\tau_{adhesive} \sim$ 0.1 KPa becomes so weak that the solidified film can be easily peeled or detached from the solid substrate at the initial retraction stage, which is characterized by capillary time scale $t_{capillary} = (\rho R_0^3/\gamma)^{1/2}$ = 8.7 ms (γ = 0.028 N/m for the surface tension of the hexadecane droplet).

Indeed, as shown in Figure 3b, the occurrence of folding times $t_{folding}$ aligns with the capillary time scale,

$$t_{folding} \simeq t_{capillary} \tag{4}$$

which likely signifies the dominant role of capillary force in the self-folding behavior.

During the folding process, the horizontal projection area ($A_{project} = \pi R_b^2$, R_b defined for the radius corresponding to an equivalent area base) of the droplet can be measured from the top-down view in experiments (inset in Figure 3c). As shown by the shadow in Figure 3c, $A_{project}/A_{max}$ decreases rapidly within 20 ms during the retraction stage and then undergoes slight changes until the droplet is completely frozen, which corresponds to the gradual transformation of polygonal wrinkling.

Hence, the mechanism of self-folding is as follows (Figure 3d). Once the droplet impacts the substrate, during the spreading stage, the thickness of the solidified film (h_{film}), which is contacted with substrate and subjected to supercooling, grows with time. Then at the instance of retraction stage at $t_{capillary}$, the film is peeled away from the substrate, since the thermal stress prevails over the adhesive stress. Because h_{film} is so thin and the film is so soft (the elastic modulus of solid

https://doi.org/10.1021/acs.nanolett.4c06529
Nano Lett. 2025, 25, 9899−9903

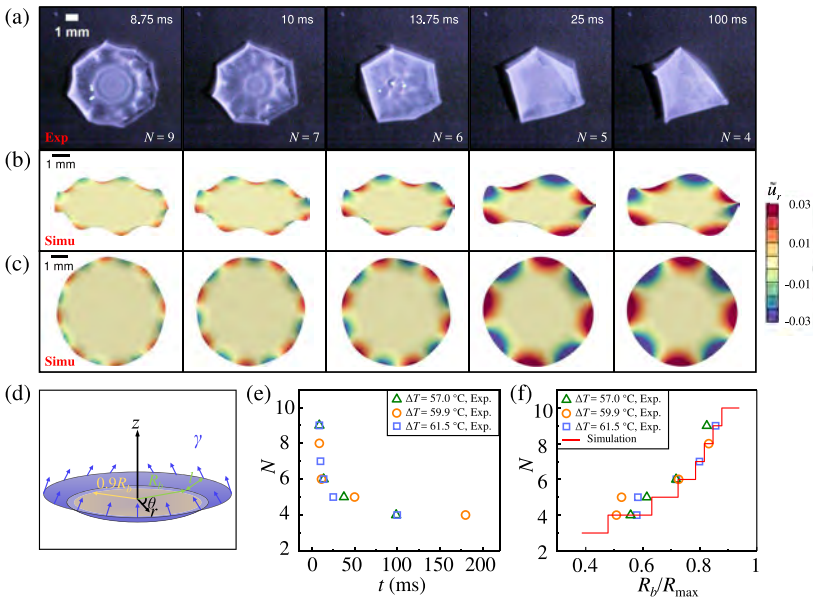

Figure 4. Polygon-wrinkling instability. (a) Snapshots of folding process for H_0 = 10 cm at strong supercooling of ΔT = 61.5 °C at T_{sub} = −43.5 °C. (b, c) Oblique view and top view for displacement ($\tilde{u}_r$) in simulation at various R_b = 2.78, 2.61, 2.38, 1.97, 1.86 mm. (d) Sketch of a thin-dish geometric model under an external load in simulations. (e) Number of wrinkles (N) as a function of time in experiments. (f) Simulations consistent with experiments for N as a function of R_b/R_{max}.

hexadecane $E \sim 100$ MPa[28,29]), the solidified film is susceptible to the deformation under the capillary force of the residual liquid. Eventually, this elasto-capillarity effect leads to the buckling instability and the wrinkled patterns. Further, this mechanism of the elasto-capillarity effect is verified by an analogous experiment of impacting a water droplet on a thin PDMS film[19,30] (Supplementary Note S3, Supplementary Movie 4) .

Polygonal Wrinkling. Different from the buckling in drying droplets of colloidal suspensions[31] or nanometer-scale hexagonal patterning at the surface of microbubbles,[32] here during the solidification process of the impacted droplet, the thin peel-off solidified film is constrained by the geometrical incompatibility as described by Gauss's *theorema egregium*, and will be subjected to the buckling instability, producing the polygonal wrinkling patterns. From the perspective of dimensional analysis, since the bending modulus of a 2D sheet, akin to a 1D slender rod, is $B \sim EH_{film}^3$, the typical elasto-capillary length (L_{ec}) is estimated by balancing surface tension energy and elastic energy,[17,19,32,33]

$$L_{ec} \sim (B/\gamma)^{1/2} \sim (EH_{film}^3/\gamma)^{1/2} \sim 1 \text{ mm} \quad (5)$$

In a similar fashion of thin-film capillary wrinkling under the capillary force exerted by a droplet placed on its surface,[20] we obtain the wavelength of wrinkling at the outer edge subjected to the internal pulling by the capillary surface from the residual liquid (λ), and the number of polygon wrinkles (N) as below,

$$\lambda \sim (L_{ec}R_b)^{1/2}, \quad N = 2\pi R_b/\lambda \sim (R_b/L_{ec})^{1/2} \quad (6)$$

Moreover, to quantitatively understand the polygon-wrinkling mode, we perform numerical simulations of the deflections of a thin-dish model under an external load[34,35] (Supplementary Note S5). The contact area between hexadecane and the substrate and the associated R_b decrease with time during the folding process, and then the number of wrinkles is reduced with time as well (Figure 4e).

For various R_b under the constrain of $R_b + l = R_{max}$ (Figure 4d), the dimensionless displacement of the r-component ($\tilde{u}_r = u_r/R_{max}$) is obtained (Figure 4b and c). Clearly, the wrinkling mode in simulations is similar to the folding pattern of the droplet for each corresponding R_b in experiments. Furthermore, the wrinkle number (N) dependent on R_b in simulations is in excellent agreement with experiments (Figure 4f).

These findings on the polygonal wrinkling of soft, solidified droplets might inspire future work to explore the complex fluid−thermal−mechanical coupling associated with advanced manufacturing for flexible electronics,[36] shape-morphing devices,[37] and soft robotics.[38]

■ ASSOCIATED CONTENT

Supporting Information

The Supporting Information is available free of charge at https://pubs.acs.org/doi/10.1021/acs.nanolett.4c06529.

Sticking pattern (MP4)
Self-peeling pattern (MP4)
Self-folding pattern (MP4)
Analogous experiment for the capillary force-driven self-folding (MP4)
Experimental methods, heat transfer model, and numerical simulations (PDF)

■ AUTHOR INFORMATION

Corresponding Authors

Man Hu − *Department of Aeronautics and Astronautics & College of Intelligent Robotics and Advanced Manufacturing, Fudan University, Shanghai 200433, China*; Email: hu.human@fudan.edu.cn

Qi Tong − *Department of Aeronautics and Astronautics & College of Intelligent Robotics and Advanced Manufacturing, Fudan University, Shanghai 200433, China*; orcid.org/0000-0003-2498-4166; Email: tong.tongqi@fudan.edu.cn

https://doi.org/10.1021/acs.nanolett.4c06529
Nano Lett. 2025, 25, 9899−9903

Daosheng Deng − *Department of Aeronautics and Astronautics & College of Intelligent Robotics and Advanced Manufacturing, Fudan University, Shanghai 200433, China*; orcid.org/0000-0002-4203-5119; Email: deng.dsdeng@fudan.edu.cn

Authors

Li Chen − *Department of Aeronautics and Astronautics & College of Intelligent Robotics and Advanced Manufacturing, Fudan University, Shanghai 200433, China*

Cheng Cao − *Department of Aeronautics and Astronautics & College of Intelligent Robotics and Advanced Manufacturing, Fudan University, Shanghai 200433, China*

Yuqi Li − *Department of Aeronautics and Astronautics & College of Intelligent Robotics and Advanced Manufacturing, Fudan University, Shanghai 200433, China*

Wenna Wu − *Department of Aeronautics and Astronautics & College of Intelligent Robotics and Advanced Manufacturing, Fudan University, Shanghai 200433, China*

Complete contact information is available at: https://pubs.acs.org/10.1021/acs.nanolett.4c06529

Author Contributions

L.C. performed the experiments and analyzed data, C.C. carried out the simulation, and L.C., C.C., Y.L, W. W, M.H., Q. T., and D.D. discussed the results. L.C., C.C., M. H., Q.T., and D.D. wrote the manuscript, Q. T. supervised the simulation model, and D.D. supervised the project.

Notes

The authors declare no competing financial interest.

■ ACKNOWLEDGMENTS

D.D. is grateful to Prof. Howard Stone for the insightful and supportive comment on this work. This work is supported by the funding from the National Program in China and startup in Fudan University.

■ REFERENCES

(1) Du, Y. H.; et al. The physics of freezing and melting in the presence of flows. *Nat. Rev. Phys.* **2024**, *6*, 676−690.
(2) Mazur, P. Freezing of living cells: mechanisms and implications. *Am. J. Physiol. Cell Physiol.* **1984**, *247*, C125.
(3) Cheng, L. N.; et al. Emerging techniques for assisting and accelerating food freezing processes: A review of recent research progresses. *Crit. Rev. Food Sci.* **2017**, *57*, 769.
(4) Kreder, M. J.; Alvarenga, J.; Kim, P.; Aizenberg, J. Design of anti-icing surfaces: smooth, textured or slippery? *Nat. Rev. Mater.* **2016**, *1*, 15003.
(5) Brodsley, L.; Frank, F. C.; Steeds, J. W. Prince Rupert's drops. *Notes Rec* **1986**, *41*, 1.
(6) Chandrasekar, S.; Chaudhri, M. M. The explosive disintegration of Prince Rupert's drops. *Philos. Mag. B* **1994**, *70*, 1195.
(7) Aben, H.; Anton, J.; Ois, M.; Viswanathan, K.; Chandrasekar, S.; Chaudhri, M. M. On the extraordinary strength of Prince Rupert's drops. *Appl. Phys. Lett.* **2016**, *109*, 231903.
(8) Kooij, S.; van Dalen, G.; Molinari, J.-F.; Bonn, D. Explosive fragmentation of Prince Rupert's drops leads to well-defined fragment sizes. *Nat. Commun.* **2021**, *12*, 2521.
(9) Gao, F. Q.; Sonin, A. A. Precise deposition of molten microdrops: the physics of digital microfabrication. *Proc. R. Soc. London A* **1994**, *444*, 533.
(10) Schiaffino, S.; Sonin, A. A. Molten droplet deposition and solidification at low Weber numbers. *Phys. Fluids* **1997**, *9*, 3172.
(11) Huerre, A.; Josserand, C.; Seon, T. Freezing and capillarity. *Annu. Rev. Fluid Mech.* **2025**, *57*, 257.
(12) Marin, A. G.; Enriquez, R.; Brunet, P.; Colinet, P.; Snoeijer, J. H. Universality of tip singularity formation in freezing water drops. *Phys. Rev. Lett.* **2014**, *113*, 054301.
(13) Ghabache, E.; Josserand, C.; Séon, T. Frozen impacted drop: From fragmentation to hierarchical crack patterns. *Phys. Rev. Lett.* **2016**, *117*, 074501.
(14) de Ruiter, J.; Soto, D.; Varanasi, K. K. Self-peeling of impacting droplets. *Nat. Phys.* **2018**, *14*, 35.
(15) Wang, F.; et al. Self-lifting droplet driven by the solidification-induced solutal Marangoni flow. *Phys. Rev. Lett.* **2024**, *132*, 014002.
(16) Style, R. W.; Jagota, A.; Hui, C. Y.; Dufresne, E. R. Elastocapillarity: Surface tension and the mechanics of soft solids. *Annu. Rev. Condens. Matter Phys.* **2017**, *8*, 99.
(17) Bico, J.; Reyssat, E.; Roman, B. Elastocapillarity: When surface tension deforms elastic solids. *Annu. Rev. Fluid Mech.* **2018**, *50*, 629.
(18) Rallabandi, B. Fluid-elastic interactions near contact at low Reynolds number. *Annu. Rev. Fluid Mech.* **2024**, *56*, 491.
(19) Py, C.; et al. Capillary origami: Spontaneous wrapping of a droplet with an elastic sheet. *Phys. Rev. Lett.* **2007**, *98*, 156103.
(20) Huang, J. H.; et al. Capillary wrinkling of floating thin polymer films. *Science* **2007**, *317*, 650.
(21) Kumar, D.; Paulsen, J. D.; Russell, T. P.; Menon, N. Wrapping with a splash: High-speed encapsulation with ultrathin sheets. *Science* **2018**, *359*, 775.
(22) Hu, M.; et al. Frozen patterns of impacted droplets: From conical tips to toroidal shapes. *Phys. Rev. Fluids* **2020**, *5*, 081601.
(23) Thievenaz, V.; et al. Retraction and freezing of a water film on ice. *Phys. Rev. Fluids* **2020**, *5*, 041601.
(24) Jin, P.; et al. Ultra-low ice-substrate adhesion and self-deicing during droplet impact freezing. *Cell Rep. Phys. Sci.* **2022**, *3*, 100894.
(25) de Ruiter, R.; et al. Contact line arrest in solidifying spreading drops. *Phys. Rev. Fluids* **2017**, *2*, 043602.
(26) Lolla, V. Y.; Ahmadi, S. F.; Park, H.; Fugaro, A. P.; Boreyko, J. B. Arrested dynamics of droplet spreading on ice. *Phys. Rev. Lett.* **2022**, *129*, 074502.
(27) Fang, W. Z.; et al. Self-peeling of frozen water droplets upon impacting a cold surface. *Commun. Phys.* **2022**, *5*, 51.
(28) Kulkarni, V.; et al. Increased solidification delays fragmentation and suppresses rebound of impacting drops. *Phys. Rev. Fluids* **2024**, *9*, 053604.
(29) Sgreva, N. R.; et al. Thermo-physical characterization of hexadecane during the solid/liquid phase change. *Thermochim. Acta* **2022**, *710*, 179180.
(30) Antkowiak, A.; et al. Instant fabrication and selection of folded structures using drop impact. *Proc. Natl. Acad. Sci. U. S. A.* **2011**, *108*, 10400.
(31) Tsapis, N.; Dufresne, E. R.; Sinha, S. S.; Riera, C. S.; Hutchinson, J. W.; Mahadevan, L.; Weitz, D. A. Onset of buckling in drying droplets of colloidal suspensions. *Phys. Rev. Lett.* **2005**, *94*, 018302.
(32) Dressaire, E.; Bee, R.; Bell, D. C.; Lips, A.; Stone, H. A. Interfacial polygonal nanopatterning of stable microbubbles. *Science* **2008**, *320*, 1198.
(33) Bico, J.; Roman, B.; Moulin, L.; Boudaoud, A. Elastocapillary coalescence in wet hair. *Nature* **2004**, *432*, 690.
(34) Choong, K. K.; Ramm, E. Simulation of buckling process of shells by using the finite element method. *Thin-Walled Struct.* **1998**, *31*, 39.
(35) Shanmugam, N. E.; Wang, C. M. *Analysis and design of plated structures: Stability*; Woodhead Publishing: 2021.
(36) Wang, Z. X.; et al. High-quality semiconductor fibres via mechanical design. *Nature* **2024**, *626*, 72.
(37) Wang, J.; Chortos, A. Performance metrics for shape-morphing devices. *Nat. Rev. Mater.* **2024**, *9*, 738.
(38) Rus, D.; Tolley, M. T. Design, fabrication and control of soft robots. *Nature* **2015**, *521*, 467.